NASA TM-81859

NASA Technical Memorandum 81859

NASA-TM-81859 19810006723

Viscous Compressible Flow About Blunt Bodies
Using a Numerically.Generated Orthogonal
Coordinate System

R. A. Graves, Jr. and H. H. Hamilton II

FOR REFERENCE

NOT TO BE TAKEN FROM THIS ROOM

July 1980

NASA

National Aeronautics and
Space Administration

Langley Research Center
Hampton, Virginia 23665

VISCOUS COMPRESSIBLE FLOW ABOUT BLUNT BODIES USING

A NUMERICALLY GENERATED ORTHOGONAL COORDINATE SYSTEM

R. A. Graves, Jr. and H. H. Hamilton II
Langley Research Center

SUMMARY

A numerical solution to the Navier-Stokes equations is obtained for blunt axisymmetric entry bodies of arbitrary shape in supersonic flow. These equations are solved on a finite-difference mesh obtained from a simple numerical technique which generates orthogonal coordinates between arbitrary boundaries. The governing equations are solved in time-dependent form using Stetter's improved stability three-step predictor-corrector method. For the present application, the metric coefficients were obtained numerically using fourth-order-accurate, finite-difference relations and proved to be totally reliable for the highly stretched mesh used to resolve the thin viscous boundary layer. Solutions are obtained for a range of blunt-body nose shapes including concavities. Results indicate that the numerically generated coordinate system performed exceptionally well and no problems were encountered in the coupling of the numerical coordinate generator and the fluid dynamic equations.

INTRODUCTION

One of the major problems retarding the rapid development of computational fluid dynamics for complex geometries has been the difficulty of generating the finite-difference mesh. Much effort has been expended to develop coordinate transformations and/or mesh generators for varying degrees of geometric complexity (see refs. 1-5 for representative examples). For viscous flow over blunted bodies, such as planetary entry vehicles, the boundary conditions on the body and the large gradients adjacent to the surface must be represented accurately by the finite-difference approximations to the Navier-Stokes equations. Toward this goal, almost all numerical solutions to the Navier-Stokes equations to date for blunt-body flows have used body geometries conducive to use with natural or nearly orthogonal coordinate systems.

In the natural coordinate system, the body surface itself forms one boundary, i.e. the body contour coincides with a constant coordinate line. Typical examples of this approach are a cylindrical coordinate system to describe flow over a cylinder, a spherical coordinate system to describe flow over a sphere, and a parabolic coordinate system to describe the flow over a paraboloidal body. Reference 6 gives a representative use of a natural coordinate system for the numerical solution of a fluid flow problem. In the natural coordinate system, the normal coordinates intersect the body orthogonally, thus simplifying the boundary conditions. There is little difficulty in compressing the mesh near the body because the computational mesh system is composed of lines parallel to the body which can be concentrated as close

to the body as desired. There is, however, one rather severe restriction on the natural coordinate system; that is, the body must have an analytic shape. Unfortunately, most planetary entry vehicles bear little resemblance to the limited number of natural coordinate systems available.

Another option is similar to the natural coordinate system in that the body surface becomes one coordinate line in the system. This is called the body-oriented coordinate system. In this system, the coordinates of a point are determined by the distance along a body surface measured from the axis of symmetry and the distance along a normal to the body. This type of system has been used to describe the flow over the forebody portions of blunt entry bodies; references 7-9 give some representative examples. Although this system has received wide use, it does suffer from several major deficiencies, one of the most serious of which is that it cannot handle body shapes with concavities (ref. 10).

Both conformal (ref. 5) and near-conformal mapping (ref. 4) have been used to generate coordinate meshes about complicated geometric shapes; however, these techniques are mathematically complicated and generally require multiple transformation steps leading to a loss of physical reality in the computational plane. Such complications make finite-difference mesh setups difficult and the computer codes generally are not easily applied/converted to general shapes.

Recently, reference 11 presented an application of a simple numerical coordinate generator (ref. 12) to blunt-body shapes. This technique allows for the numerical generation of general orthogonal coordinate systems about a wide range of body geometries. In this technique, the body can be represented by a series of discrete (but continuous) points rather than by an analytical approximation, and in the transformed computational plane, the region of interest is rectangular with the body surface being a coordinate line. This representation combines the advantages of the natural coordinate system and the body-oriented coordinate system. An additional advantage is that the coordinates are generated in the physical plane, which simplifies the finite-difference mesh setup. This technique was used in a time-dependent solution procedure for inviscid flow over blunt bodies (ref. 13). The use of the time-dependent solution procedure, where the moving shock wave was the outer-coordinate boundary, required that the coordinate system be regenerated at the end of each time step. This coupling of the fluid dynamics and the coordinate system worked very well for a large number of test cases. However, this application was for inviscid flow only and the finite-difference meshes were nearly equally spaced.

The present analysis uses the coordinate generation technique (ref. 11) along with the time-dependent solution concepts (ref. 13) to obtain solutions to the full Navier-Stokes equations for viscous compressible flow over blunt bodies. The emphasis is on obtaining fluid-flow solutions for blunt bodies of varying nose shapes (complexity) where the mesh must be highly compressed to resolve the viscous boundary layer.

a_2, a_3	forebody shape coefficients
C_1, C_2	Sutherland's viscosity coefficients
C_p	specific heat
E	average error
f	arbitrary function
F	arbitrary vector function
h	static enthalpy
$h_{i,j}$	metrical coefficients
$h_{1_j} h_{2_j} h_{3_j}$	transformed coordinate metrics
i	ζ direction index
I	total intervals in ζ direction
j	η direction index
J	total intervals in η direction
K_c	spacing parameter
M	Mach number
N	unequal spacing coordinate parameter
N_{pr}	Prandtl number
N_{R_e}	Reynolds number
p	pressure
q	nondimensional heat transfer, $q = \bar{q}/\bar{\rho}_\infty \bar{V}_\infty^3$
R_N	nose radius, m
r_1	local distance between body surface and outer boundary
r_s	radius of body surface
S_1	cotangent of body angle at tangency point
t	nondimensional time, $t = \bar{t}\, \bar{V}_\infty/R_N$

T	nondimensional temperature, $T = \bar{T}\,\bar{C}_{p_\infty}/\bar{V}_\infty^2$
U	arbitrary vector
u	nondimensional tangential velocity, $u = \bar{u}/\bar{V}_\infty$
V	free-stream velocity, m/s
^sV	nondimensional normal velocity, $^sV = {}^s\bar{V}/\bar{V}_\infty$
V	nondimensional normal velocity, $V = \bar{V}/\bar{V}_\infty$
X,Y	Cartesian coordinates
$^sX,{}^sY$	shock location in Cartesian coordinates
Z	axial coordinate
α	arbitrary parameter in Stetter's method
β	shock angle
γ	ratio of specific heats
ε	convergence criteria
η	transformed normal coordinate
θ_s	body-surface angle (see fig. 1)
θ_1	local angle (see fig. 1)
θ_c	cone angle
u	nondimensional viscosity, $u = \bar{u}/u_\infty$
ξ	transformed tangential coordinate
ρ	nondimensional density, $\rho = \bar{\rho}/\rho_\infty$
$\hat{\rho}$	radial distance (see fig. 5)
σ	damping coefficient

Superscripts:

⁻	dimensional values

Subscripts:

∞	free-stream quantities

4

METHOD OF ANALYSIS

Coordinate System

The numerically generated orthogonal coordinates will be determined from the original X,Y coordinate system's description of the body surface and shock wave. Taking the origin of the X,Y system as lying inside the body to be described, the surface distance ξ, which forms one of the transformed orthogonal coordinates, can be calculated by defining ξ as zero on the -X axis (fig. 1) and increasing to unity at the end of the forebody surface. Thus ξ is given by

$$\xi(\theta_s) = \frac{\int_0^{\theta_s} \left[r_s^2 + \left[\left(\frac{dr_s}{d\theta_s} \right)^2 \right] \right]^{1/2} d\theta}{\int_0^{\theta_e} \left[r_s^2 + \left[\left(\frac{dr_s}{d\theta_s} \right)^2 \right] \right]^{1/2} d\theta}$$

where $r_s = (X_s^2 + Y_s^2)^{1/2}$ and $\theta_s = \cos^{-1}(-X_s/r_s)$. As in the analysis of reference 13, the shock wave is taken as the outer boundary of the transformed coordinate system. On the outer boundary, $\eta = 1$ while on the body surface, $\eta = 0$. The level lines between the outer boundary, shock wave, and the body surface can be constructed along straight lines connecting corresponding points on the body and shock. Note that the mesh points on the outer boundary are not the final mesh points, but initial values used only to set up the level lines. The actual mesh points will result from the numerical generation of the orthogonal normal lines. The spacing of the level lines is arbitrary; however, for viscous flows, the boundary layer must be resolved and the unequal spacing relation of reference 14 can be easily applied,

$$\eta_j = \frac{K_c^{N_j/\Delta N} - 1}{K_c^{1/\Delta N} - 1}$$

where $N_j = (j-1)\Delta N$ and $N_J = 1.$, with $\Delta N = 1/(J-1)$ and K_c being the spacing parameter (generally $1 < K_c < 2$). The larger the spacing parameter K_c, the more unequal the spacing. Using the unequal spacing relation, the level lines between all corresponding points on the body and shock can be calculated. The relationships for the corresponding values of X,Y can be obtained (see fig. 1 for geometrical schematic) from

$$r_{1,i} = [(X_{\eta=1} - X_{\eta=0})_i^2 + (Y_{\eta=1} - Y_{\eta=0})_i^2]^{1/2}$$

$$X_{i,j} = X_{i,\eta=0} + (\eta_j r_{1,i}) \cos \theta_1$$

$$Y_{i,j} = Y_{i,\eta=0} + (\eta_j r_{1,i}) \sin \theta_1$$

5

where

$$\theta_1 = \sin^{-1}[(Y_{i,\eta=1} - Y_{i,\eta=0})/r_{1,i}].$$

Figure 2 shows the level lines constructed in this manner for a spherically capped conical body with $K_c = 1.01$, which gives nearly equal spacing.

Once the level lines have been determined, the normal lines are constructed numerically so that an orthogonal system is defined. The approach to the construction of the normal lines is the one given in reference 12 which uses a simple "predictor-corrector" technique analogous to the trapezoidal integration method of numerical integration. In this technique, the solution is first predicted from the level line at a known point by using the Euler method. Once the predicted point on the next level line is obtained, the slope at that point is calculated and a new predicted point is obtained using this slope. The actual solution is then a combination of these two solutions, i.e. the final X,Y values are an average of the predicted and corrected ones. This procedure is illustrated in figure 3. Starting on the body, the solution proceeds point by point along a level line until all normals on that level have been constructed. Then the solution proceeds to the next level and the process is continued until the outer boundary shock is reached. Figure 4 shows a typical orthogonal coordinate mesh constructed about a spherically capped conical body.

Coordinate Metrics

Once the coordinate system is constructed, then the X,Y location of all mesh points is known and using the coordinate system depicted in figure 5, the metric coefficients can be determined using the nomenclature of reference 15.

$$u^1 = \eta \qquad\qquad x^1 = \hat{\rho} \cos \phi$$

$$u^2 = \xi \qquad\qquad x^2 = \hat{\rho} \sin \phi$$

$$u^3 = \phi \qquad\qquad x^3 = z$$

Note that $\hat{\rho} = \hat{\rho}(\xi,\eta)$ and $z = z(\xi,\eta)$. The metric coefficients are obtained from

$$h_{i,j} = \frac{\partial x^1}{\partial u^i}\frac{\partial x^1}{\partial u^j} + \frac{\partial x^2}{\partial u^i}\frac{\partial x^2}{\partial u^j} + \frac{\partial x^3}{\partial u^i}\frac{\partial x^3}{\partial u^j}$$

For an orthogonal system, the metric coefficients $h_{1,2}$, $h_{2,1}$, $h_{1,3}$, $h_{3,1}$, $h_{2,3}$, and $h_{3,2}$ all have to be zero, leaving only the three familiar coefficients h_1, h_2, h_3.

$$h_1 = \sqrt{h_{1,1}} \qquad h_2 = \sqrt{h_{2,2}} \qquad h_3 = \sqrt{h_{3,3}}$$

6

When the derivatives in the metric coefficient relation are taken, the following metric coefficient expressions are obtained:

$$h_{1,1} = (\frac{\partial \hat{\rho}}{\partial \eta})^2 + (\frac{\partial z}{\partial \eta})^2$$

$$h_{1,2} = h_{2,1} = \frac{\partial \rho}{\partial \eta} \frac{\partial \hat{\rho}}{\partial \xi} + \frac{\partial z}{\partial \eta} \frac{\partial z}{\partial \xi}$$

$$h_{1,3} = h_{3,1} = 0$$

$$h_{2,2} = (\frac{\partial \hat{\rho}}{\partial \xi})^2 + (\frac{\partial z}{\partial \xi})^2$$

$$h_{2,3} = h_{3,2} = 0$$

$$h_{3,3} = \hat{\rho}^2$$

With the choice of the present coordinate system, two of the three necessary orthogonality conditions are identically satisfied, leaving only the $h_{1,2}$ coefficient, which was shown in reference 11 to be negligible for the present application. Thus, only the three necessary metrics are left:

$$h_1 = [(\frac{\partial \hat{\rho}}{\partial \eta})^2 + (\frac{\partial z}{\partial \eta})^2]^{1/2}$$

$$h_2 = [(\frac{\partial \hat{\rho}}{\partial \xi})^2 + (\frac{\partial z}{\partial \xi})^2]^{1/2}$$

$$h_3 = \hat{\rho}$$

Since the computational plane (ξ,η) is an equally spaced rectangular region (see fig. 6), the derivatives in the above metric coefficient relations can be evaluated using equally spaced, central finite differences. For the present analysis, fourth-order-accurate relations (ref. 16) are used in place of simpler second-order-accurate finite differences in order to produce smoothly varying metric coefficients adjacent to the stagnation line. These fourth-order-accurate metric coefficients proved to be totally satisfactory for the present analysis even in the regions of high-mesh stretching/compression.

Governing Equations

The equations used in the present analysis are the full unsteady Navier-Stokes equations in general orthogonal coordinates for laminar viscous flow as given by reference 17. These equations in nondimensional form are:

$$\frac{\partial \rho}{\partial t} = -\frac{u}{h_1} \frac{\partial \rho}{\partial \xi} - \frac{v}{h_2} \frac{\partial \rho}{\partial \eta} - \frac{\rho}{h_1} \frac{\partial u}{\partial \xi} - \frac{\rho}{h_2} \frac{\partial v}{\partial \eta}$$

$$- \frac{\rho u}{h_1 h_2 h_3} \frac{\partial}{\partial \xi} (h_2 h_3) - \frac{\rho v}{h_1 h_2 h_3} \frac{\partial}{\partial \eta} (h_1 h_3)$$

7

$$\frac{\partial u}{\partial t} = - \frac{u}{h_1} \frac{\partial u}{\partial \xi} - \frac{v}{h_2} \frac{\partial u}{\partial \eta} - \frac{uv}{h_1 h_2} \frac{\partial h_1}{\partial \eta} + \frac{v^2}{h_1 h_2} \frac{\partial h_2}{\partial \xi} - \frac{1}{h_1} \frac{\partial \rho}{\partial \xi}$$

$$+ \frac{1}{\rho N_{R_e}} \left\{ \frac{1}{h_1 h_2 h_3} \left[\frac{\partial}{\partial \xi} (h_2 h_3 \tau_{\xi\xi}) + \frac{\partial}{\partial \eta} (h_1 h_3 \tau_{\xi\eta}) \right] \right.$$

$$\left. + \frac{\tau_{\xi\eta}}{h_1 h_2} \frac{\partial h_1}{\partial \eta} - \frac{\tau_{\eta\eta}}{h_1 h_2} \frac{\partial h_2}{\partial \xi} - \frac{\tau_{\phi\phi}}{h_1 h_3} \frac{\partial h_3}{\partial \xi} \right\}$$

$$\frac{\partial v}{\partial t} = - \frac{u}{h_1} \frac{\partial v}{\partial \xi} - \frac{v}{h_2} \frac{\partial v}{\partial \eta} - \frac{vu}{h_1 h_2} \frac{\partial h_2}{\partial \xi} + \frac{u^2}{h_1 h_2} \frac{\partial h_1}{\partial \eta} - \frac{1}{\rho h_2} \frac{\partial \rho}{\partial \eta}$$

$$+ \frac{1}{\rho N_{R_e}} \left\{ \frac{1}{h_1 h_2 h_3} \left[\frac{\partial}{\partial \xi} (h_2 h_3 \tau_{\xi\eta}) + \frac{\partial}{\partial \eta} (h_1 h_3 \tau_{\eta\eta}) \right] \right.$$

$$\frac{\partial h}{\partial t} = - \frac{u}{h_1} \frac{\partial h}{\partial \xi} - \frac{v}{h_2} \frac{\partial h}{\partial \eta} + \frac{u}{\rho h_1} \frac{\partial \rho}{\partial \xi} + \frac{v}{\rho h_2} \frac{\partial \rho}{\partial \eta}$$

$$+ \frac{1}{h_1 h_2 h_3 N_{Re} N_{Pr}} \left\{ \frac{\partial}{\partial \xi} \left(\frac{h_2 h_3 \mu}{h_1} \frac{\partial h}{\partial \xi} \right) \right.$$

$$\left. + \frac{\partial}{\partial \eta} \left(\frac{h_1 h_3 \mu}{h_2} \frac{\partial h}{\partial \eta} \right) \right\} + \frac{1}{\rho N_{R_e}} \left\{ \frac{\tau_{\xi\xi}}{h_1} \frac{\partial u}{\partial \xi} \right.$$

$$+ v \left[\frac{\tau_{\xi\xi}}{h_1 h_2} \frac{\partial h_1}{\partial \eta} + \frac{\tau_{\phi\phi}}{h_2 h_3} \frac{\partial h_3}{\partial \eta} - \frac{\tau_{\xi\eta}}{h_1 h_2} \frac{\partial h_2}{\partial \xi} \right]$$

$$+ u \left[\frac{\tau_{\eta\eta}}{h_1 h_2} \frac{\partial h_2}{\partial \xi} + \frac{\tau_{\phi\phi}}{h_1 h_3} \frac{\partial h_3}{\partial \xi} - \frac{\tau_{\xi\eta}}{h_1 h_2} \frac{\partial h_1}{\partial \eta} \right]$$

$$\left. + \frac{\tau_{\eta\eta}}{h_2} \frac{\partial v}{\partial \eta} + \frac{\tau_{\xi\eta}}{h_2} \frac{\partial u}{\partial \eta} + \frac{\tau_{\xi\eta}}{h_1} \frac{\partial v}{\partial \xi} \right\}$$

where

$$\tau_{\xi\xi} = - \frac{2\mu}{3} (\nabla \cdot \vec{v}) + \mu e_{\xi\xi}$$

$$\tau_{\eta\eta} = - \frac{2\mu}{3} (\nabla \cdot \vec{v}) + \mu e_{\eta\eta}$$

$$\tau_{\phi\phi} = -\frac{2\mu}{3} (\nabla \cdot \vec{v}) + \mu e_{\phi\phi}$$

$$\tau_{\xi\eta} = \tau_{\eta\xi} = \mu e_{\xi\eta}$$

$$\nabla \cdot \vec{v} = \frac{1}{h_1 h_2 h_3} \left[\frac{\partial}{\partial \xi} (h_2 h_3 u) + \frac{\partial}{\partial \eta} (h_1 h_3 v) \right]$$

$$e_{\xi\xi} = \frac{2}{h_1} \frac{\partial u}{\partial \xi} + \frac{2v}{h_1 h_2} \frac{\partial h_1}{\partial \eta}$$

$$e_{\eta\eta} = \frac{2}{h_2} \frac{\partial v}{\partial \eta} + \frac{2u}{h_1 h_2} \frac{\partial h_2}{\partial \xi}$$

$$e_{\phi\phi} = \frac{2u}{h_1 h_3} \frac{\partial h_3}{\partial \xi} + \frac{2v}{h_2 h_3} \frac{\partial h_3}{\partial \eta}$$

$$e_{\xi\eta} = \frac{h_2}{h_1} \frac{\partial}{\partial \xi} \left(\frac{v}{h_2} \right) + \frac{h_1}{h_2} \frac{\partial}{\partial \eta} \left(\frac{u}{h_1} \right)$$

The axis of symmetry, stagnation line, is a singular line in the computational domain because $h_3 = 0$ and $u = 0$ along the axis. The limiting forms are:

$$\frac{\partial \rho}{\partial t} = -\frac{2}{h_1} \rho \frac{\partial u}{\partial \xi} - \frac{1}{h_2} \frac{\partial}{\partial \eta} (\rho v) - \rho v \left[\frac{1}{h_2 \frac{\partial h_3}{\partial \xi}} \frac{\partial}{\partial \eta} \left(\frac{\partial h_3}{\partial \xi} \right) + \frac{1}{h_1 h_2} \frac{\partial h_1}{\partial \eta} \right]$$

$$\frac{\partial v}{\partial t} = -\frac{v}{h_2} \frac{\partial v}{\partial \eta} - \frac{1}{\rho h_2} \frac{\partial \rho}{\partial \eta} + \frac{1}{\rho N_{Re}} \left\{ \frac{2}{h_1} \frac{\partial \tau_{\xi\eta}}{\partial \xi} \right.$$

$$+ \frac{1}{h_2} \frac{\partial \tau_{\eta\eta}}{\partial \eta} + \tau_{\eta\eta} \left[\frac{1}{h_1 h_2} \frac{\partial h_1}{\partial \eta} + \frac{1}{h_2 \frac{\partial h_3}{\partial \xi}} \frac{\partial}{\partial \eta} \left(\frac{\partial h_3}{\partial \xi} \right) \right]$$

$$\left. - \tau_{\xi\xi} \frac{1}{h_1 h_2} \frac{\partial h_1}{\partial \eta} \right\}$$

$$\frac{\partial h}{\partial t} = -\frac{v}{h_2}\frac{\partial h}{\partial \eta} + \frac{v}{\rho h_2}\frac{\partial \rho}{\partial \eta} + \frac{2}{\rho h_1 h_2 N_{Re} N_{Pr}}\frac{\partial}{\partial \xi}\left(\frac{h_2 \mu}{h_1}\frac{\partial h}{\partial \xi}\right)$$

$$+ \frac{1}{\rho h_1 h_2 N_{Re} N_{Pr}}\frac{\partial}{\partial \eta}\left(\frac{h_1 \mu}{h_2}\frac{\partial h}{\partial \eta}\right)$$

$$+ \frac{1}{\rho h_1 h_2 N_{Re} N_{Pr}}\left[\frac{\mu\, h_1}{h_2 \frac{\partial h_3}{\partial \xi}}\frac{\partial}{\partial \eta}\left(\frac{\partial h_3}{\partial \xi}\right)\right]\frac{\partial h}{\partial \eta}$$

$$+ \frac{1}{\rho N_{Re}}\left\{\frac{2\tau_{\xi\xi}}{h_1}\frac{\partial u}{\partial \xi} + \bar{v}\left[\frac{\tau_{\xi\xi}}{h_1 h_2}\frac{\partial h_1}{\partial \eta} + \frac{\tau_{\phi\phi}}{h_2 \frac{\partial h_3}{\partial \xi}}\frac{\partial}{\partial \eta}\left(\frac{\partial h_3}{\partial \xi}\right)\right]\right.$$

$$\left. + \frac{\tau_{\eta\eta}}{h_2}\frac{\partial v}{\partial \eta}\right\}$$

where

$$\tau_{\xi\xi} = -\frac{2\mu}{3}(\nabla \cdot \vec{v}) + \mu e_{\xi\xi}$$

$$\tau_{\eta\eta} = -\frac{2\mu}{3}(\nabla \cdot \vec{v}) + \mu e_{\eta\eta}$$

$$\tau_{\phi\phi} = -\frac{2\mu}{3}(\nabla \cdot \vec{v}) + \mu e_{\phi\phi}$$

$$e_{\xi\xi} = \frac{2}{h_1}\frac{\partial u}{\partial \xi} + \frac{2v}{h_1 h_2}\frac{\partial h_1}{\partial \eta}$$

$$e_{\eta\eta} = \frac{2}{h_2}\frac{\partial v}{\partial \eta}$$

$$e_{\phi\phi} = \frac{2v}{h_2 \frac{\partial h_3}{\partial \xi}}\frac{\partial}{\partial \eta}\left(\frac{\partial h_3}{\partial \xi}\right) + \frac{2}{h_1}\frac{\partial u}{\partial \xi}$$

$$\nabla \cdot \vec{v} = \frac{2}{h_1}\frac{\partial u}{\partial \xi} + \frac{1}{h_2}\frac{\partial v}{\partial \eta} + v\left[\frac{1}{h_1 h_2}\frac{\partial h_1}{\partial \eta} + \frac{1}{h_2 \frac{\partial h_3}{\partial \xi}}\frac{\partial}{\partial \eta}\left(\frac{\partial h_3}{\partial \xi}\right)\right]$$

In addition to the above conservation equations, an equation of state and a viscosity law must be specified. For a perfect gas, the equation of state can be given by

$$p = \frac{\gamma-1}{\gamma}\rho h$$

and Sutherland's viscosity equation is used in the form

$$\mu = C_1 \frac{\bar{T}^{3/2}}{C_2 + \bar{T}}$$

to determine the molecular (laminar) viscosity.

Boundary Conditions

Along the body surface for the present analysis, the following conditions are imposed:

$$u = 0 \quad \text{(no slip)}$$

$$v = 0 \quad \text{(no blowing)}$$

$$h = h_w \quad \text{(constant wall temperature)}$$

$$\left.\frac{dp}{d\eta}\right)_N = 0, \quad P_{i,1} = \left[\left(4p_{i,2} - p_{i,3}\right)/3\right]$$

Because the flow analysis is in the unsteady form, both the flow properties and shock velocity have to be specified at the upper boundary. This is accomplished using a modified form of the Rankine-Hugoniot relations, a complete development of which can be found in reference 13. In order to apply these relations, the pressure immediately behind the shock has to be calculated using only quantities interior to the computational region. This calculation is performed using the continuity equation, energy equation, and equation of state with the appropriate derivatives in these equations being expressed by backward finite differences. Once the shock velocity is obtained at each mesh point along the shock, the shock position is determined from the solution of the following equations:

$$\frac{d^S X_i}{dt} = {}^S V_i \cos(\pi/2 - \beta)$$

$$\frac{d^S Y_i}{dt} = -{}^S V_i \sin(\pi/2 - \beta)$$

The flow conditions along the outflow boundary are obtained using the following second-order-accurate extrapolation relation for equally spaced data (ref. 7):

$$f_i = (20f_{i-1} - 6f_{i-2} - 4f_{i-3} + f_{i-4})/11 + O(\Delta\xi^2)$$

Numerical Method of Solution

Because of the necessity of recalculating the orthogonal coordinate system at each time step (due to the shock movement), it is imperative that the overall solution converge as rapidly as possible to minimize the additional work. For this reason, Stetter's method (ref. 18) is chosen as the method of solution, for it has been demonstrated (refs. 19 and 20) to have an expanded region of stability which allows for a more rapid marching to steady state. In Stetter's three-step predictor-corrector method, the derivatives in the governing equations are expressed as second-order finite differences so that the overall solution is of second-order accuracy in the space dimensions. Since the steady-state solution is the desired end product, the dp/dt term in the energy equation is dropped (refs. 7 and 9) and thus temporal accuracy is not maintained.

In order to facilitate the use of Stetter's method, the governing equations are recast in the following simplified form:

$$\frac{\partial U}{\partial t} = F$$

$$U = \begin{Bmatrix} \rho \\ u \\ v \\ h \\ s_X \\ s_Y \end{Bmatrix}$$

and F represents the righthand side of the appropriate equation.

The three-step process becomes:

$$^{(0)}U_{i,j}^{N+1} = U_{i,j}^N + \Delta t_k\, F_{i,j}^N \qquad \text{(step 1)}$$

$$^{(1)}U_{i,j}^{N+1} = U_{i,j}^N + \frac{\Delta ti}{2}\, (^{(0)}F_{i,j}^{N+1} + F_{i,j}^N) \qquad \text{(step 2)}$$

$$^{(2)}U_{i,j}^{N+1} = U_{i,j}^N + \frac{\Delta ti}{2}\, (^{(1)}F_{i,j}^{N+1} + F_{i,j}^N) \qquad \text{(step 3)}$$

$$U_{i,j}^{N+1} + \alpha\, {}^{(1)}U_{i,j}^{N+1} + (1-\alpha)\, {}^{(2)}U_{i,j}^{N-1} \qquad \text{(parameterization)}$$

After the parameterization step, a damping (or smoothing) of the solution is performed to prevent oscillations in the flow from destroying the solution process. This damping is the fourth-order procedure given in reference 21 and used quite successfully in references 9 and 10.

Because of the large variation in grid spacing used in the present analysis, the local maximum time step based on the CFL condition could not be used as was done in reference 20. Instead, a local minimum time step was found along each ξ = constant line and then the time step was defined as

$$\Delta t_i = 2.4 \left[\underset{2 \leq j \leq J}{\text{Min}} \left(\Delta t_{CFL,j} \right) \right]_{i=\text{constant}}$$

This time step proved entirely satisfactory for the range of body shapes given in the present analysis.

The orthogonal coordinate system was numerically generated at the end of each full time step while at the end of steps 1 and 2, only the shock position and related metrics were calculated. This is the same procedure used in reference 13 where a wide variety of inviscid blunt-body flow fields were calculated. Note that in the present study, no attempt was made to optimize the fluid dynamic/orthogonal coordinate calculation procedure.

The solution procedure was assumed to be converged (at steady state) when the average error was less than the convergence criteria. The average error is defined as

$$E = \frac{\left\{ \sum\limits_{i=1}^{I-1} \sum\limits_{j=2}^{J-1} \left| \dfrac{\rho_{i,j}^{N+1} - \rho_{i,j}^{N}}{\rho_{i,j}^{N}} \right| \right\}}{(I-1)(J-2)}$$

Thus, the solution is converged when

$$E < \varepsilon$$

where ε is a small value on the order of 10^{-6}.

RESULTS AND DISCUSSION

The present analysis was used to calculate the flow over a 45° hyperboloid using the test conditions given in table 1. The computational grid was a 15 × 31 mesh with a spacing parameter $K_c = 1.2$ in the η direction, which gives a highly compressed mesh adjacent to the body surface. The spacing parameter for the ξ direction was $K_c = 1.15$, which gave a slight compression in the stagnation region and a stretching of the mesh toward the outflow boundary. The calculated pressure and heat-transfer distributions are given in figures 7 and 8 where an excellent comparison with two other computational solutions is seen. The present analysis had no difficulty in handling this analytic body with its smooth variation in surface curvature.

13

The body-oriented coordinate system which has received very wide use because of its simplicity suffers several serious deficiencies, one of the more serious of which is that for bodies with a curvature discontinuity, such as spherically capped cones, there results a singularity in the governing equations. This problem can be circumvented by making the discontinuity point a special case (ref. 22) where special derivative relations are applied. However, the present numerically generated coordinate system does not suffer the same problem and this was amply demonstrated for inviscid flow (ref. 13) where solutions for a number of curvature discontinuous bodies were obtained for a wide range of conditions. Using the present analysis, the flow over a 45° spherically capped conical body was calculated using the condition of table 1. The computed heat-transfer distribution is plotted in figure 9 along with both experimental and computational results. Again, the comparisons are very good and the present analysis had no difficulty in handling the surface curvature discontinuity.

A more rigorous demonstration of the capabilities of the numerical orthogonal coordinate generator can be seen on bodies with increasing nose bluntness, including those with reverse curvature. A family of bodies having these properties will be generated using the following cubic forebody generator:

$$X = X_o + a_2 Y^2 + a_3 Y^3$$

where

$$a_2 = \frac{3}{Y_1^2} X_1 - X_o - \frac{s_1 Y_1}{3}$$

$$a_3 = (s_1 - 2a_2 Y_1)/3Y_1^2$$

$$s_1 = \frac{1}{\tan \theta_c}$$

$$X_1 = 0.5$$

$$Y_1 = 1.$$

$$\theta_c = 40°$$

The forebody joins smoothly to the conical afterbody with the surface angle specified by θ_c. Figure 10 gives the forebody shapes as a function of X_o and these five shapes represent the range of shapes that could be expected for planetary entry bodies experiencing severe ablation in the stagnation region (ref. 23). Using the conditions of table 1, but with $\sigma = 0.003$, the flow fields about the five body shapes were computed. The pressure and heat-transfer distributions are given in figures 11 and 12 where the effect of nose blunting is readily apparent. Also, the representative effects of blunting on shock and sonic-line shape can be seen in figures 13-15.

14

A representative converged coordinate mesh is given in figure 16 for the $X_0 = 0.4$ body. Note the highly compressed mesh near the body surface which was necessary to resolve the boundary layer. All these results obtained with the present analysis are excellent with no noted undesirable flow-field/coordinate system coupling effects. Part of the success of the present analysis is due to the smooth metric coefficients produced by the fourth-order differencing. Table 2 gives the metric coefficients at two locations for the $X_0 = 0.4$ case and these results are typical of all the solutions obtained with the present analysis.

CONCLUDING REMARKS

The use of numerically generated orthogonal coordinates in compressible viscous-flow solutions to the Navier-Stokes equations is both practical and desirable. The technique has been demonstrated for a range of blunt-body shapes and the use of numerically evaluated metric coefficients has been successfully demonstrated. Although the present analysis had a moving boundary which necessitated recalculating the coordinate system at each step of the flow calculation, the technique should find easy application in static coordinate situations.

REFERENCES

1. Amsden, A. A. and Hirt, C. W.: A Simple Scheme for Generating General Curvilinear Grids. J. of Comput. Phys., vol. 11, no. 3, March 1973, pp. 348-359.

2. Starius, Göran: Constructing Orthogonal Curvilinear Meshes by Solving Initial Value Problems. Numer. Math., vol. 28, fasc. 1, 1977, pp. 25-48.

3. Gnoffo, Peter A.: A Generalized Orthogonal Coordinate System for Describing Families of Axisymmetric and Two-Dimensional Bodies. NASA TM X-3468, 1977.

4. Thompson, Joe F.; Thames, Frank C.; and Mastin, C. Wayne: Automatic Numerical Generation of Body-Fitted Curvilinear Coordinate System for Field Containing Any Number of Arbitrary Two-Dimensional Bodies. J. Comput. Phys., vol. 15, no. 3, July 1974, pp. 299-319.

5. Ives, David C.: A Modern Look at Conformal Mapping Including Multiple Connected Regions. AIAA Journal, vol. 14, no. 8, August 1976, pp. 1006-1011.

6. Peyret, Roger and Viviand, Henri: Calculation of the Flow of a Viscous Compressible Fluid Around an Obstacle of Parabolic Shape. NASA TT F-16558, 1975.

7. Graves, Randolph A., Jr.: Solutions to the Navier-Stokes Equations for Supersonic Flow Over Blunt Bodies With Massive Wall Blowing. DSc. Dissertation, George Washington University, Washington, DC, November 1977.

8. Davis, R. T.: Numerical Solution of the Hypersonic Viscous-Shock-Layer Equations. AIAA Journal, vol. 8, no. 5, May 1970.

9. Kumar, Ajay and Graves, R. A., Jr.: Numerical Solution of the Viscous Hypersonic Flow Past Blunted Cones at Angle of Attack. AIAA Paper 77-172, January 1977.

10. Gnoffo, P. A.: Solutions to the Navier-Stokes Equations for Supersonic Flow Over Blunt Bodies in a Generalized Orthogonal Coordinate System. M.S. Thesis, George Washington University, Washington, DC, April 1977.

11. Graves, Randolph A., Jr.: Application of a Numerical Orthogonal Coordinate Generator to Axisymmetric Blunt Bodies. NASA TM 80131, October 1979.

12. McNally, William D.: FORTRAN Program for Generating a Two-Dimensional Orthogonal Mesh Between Two Arbitrary Boundaries. NASA TN D-6766, 1972.

13. Hamilton, H. H., II and Graves, R. A., Jr.: Application of a Numerically Generated Orthogonal Coordinate System to the Solution of Inviscid Axisymmetric Supersonic Flow Over Blunt Bodies. NASA TP 1619, January 1980.

14. Blottner, F. G.: Variable Grid Scheme Applied to Turbulent Boundary Layers. Comput. Methods Appl. Mech. & Eng., vol. 4, no. 2, September 1974, pp. 179-194.

15. Wills, A. P.: Vector Analysis With an Introduction to Tensor Analysis. Dover Publ., Inc., 1958.

16. Milne, W. E.: Numerical Calculus. Princeton University Press, Princeton, New Jersey, 1949.

17. Back, L. H.: Conservation Equations of a Viscous, Heat-Conducting Fluid in Curvilinear Orthogonal Coordinates. JPL Technical Report 32-1332, September 1968.

18. Stetter, H. J.: Improved Absolute Stability of Predictor-Corrector Schemes. Computing, vol. 3, 1968, p. 286.

19. Graves, R. A., Jr. and Johnson, N. E.: Navier-Stokes Solutions Using Stetter's Method. AIAA Journal, vol. 16, September 1978, pp. 1013-1015.

20. Kumar, Ajay and Graves, R. A., Jr.: Comparative Study of the Convergence Rates of Two Numerical Techniques. AIAA Journal, vol. 16, November 1978, pp. 1214-1216.

21. Barnwell, R. W.: A Time-Dependent Method for Calculating Supersonic Angle-of-Attack Flow About Axisymmetric Blunt Bodies With Sharp Shoulders and Smooth Nonaxisymmetric Blunt Bodies. NASA TN D-6283, August 1971.

16

22. Srivastava, B. N.: Viscous-Shock-Layer Solutions for Hypersonic Sphere
    Cones. Ph.D. Dissertation, University of Cincinnati, Cincinnati,
    Ohio, November 1976.

23. Sutton, Kenneth: Effect of Probe Configuration on Radiative Heating
    During Jovian Entry. AIAA Paper No. 76-471, July 1976.

TABLE 1.- COMPUTATIONAL TEST CONDITIONS

$$M_\infty = 10.33$$

$$\gamma = 1.4$$

$$P_\infty = 100.77 \text{ N/m}^2$$

$$T_\infty = 46.26° \text{ K}$$

$$T_w = 330.6° \text{ K}$$

$$R_N = 0.03175 \text{ m}$$

$$N_{Re} = 115600$$

$$\varepsilon = 2.5 \times 10^{-6}$$

$$\sigma = 0.001$$

$$N_{pr} = 0.7$$

TABLE 2.- METRIC COEFFICIENTS

(a) Tangential Direction Variations

$\eta = .1333$			
ξ	h_1	h_2	h_3
0	1.0427	.00861	0
.0714	1.1042	.00851	.0756
.1428	1.2241	.00818	.1578
.2143	1.3472	.00765	.2471
.2857	1.4831	.00693	.3447
.3571	1.6337	.00608	.4528
.4286	1.7970	.00522	.5740
.5000	1.9680	.00461	.7076
.5714	2.1608	.00458	.8344
.6428	2.3878	.00525	.9687
.7143	2.6284	.00626	1.0847
.7857	2.8881	.00706	1.2112
.8571	3.1767	.00763	1.3504
.9286	3.4944	.00800	1.5035
1.0000	3.8438	.00821	1.6718

TABLE 2.- METRIC COEFFICIENTS (CONCLUDED)

(b) Normal Direction Variations

$\xi = .3571$			
η	h_1	h_2	h_3
0	1.6329	.00249	.4529
.0333	1.6331	.00311	.4529
.0667	1.6332	.00389	.4529
.1000	1.6334	.00486	.4529
.1333	1.6337	.00608	.4529
.1667	1.6340	.00759	.4528
.2000	1.6344	.00949	.4528
.2333	1.6349	.01187	.4527
.2667	1.6355	.01485	.4526
.3000	1.6363	.01856	.4525
.3333	1.6373	.02321	.4524
.3667	1.6385	.02902	.4522
.4000	1.6401	.03629	.4520
.4333	1.6420	.04539	.4518
.4667	1.6444	.05679	.4515
.5000	1.6474	.07105	.4512
.5333	1.6512	.08891	.4507
.5667	1.6559	.11129	.4502
.6000	1.6617	.13933	.4495
.6333	1.6690	.17449	.4487
.6667	1.6781	.21862	.4477
.7000	1.6894	.27398	.4466
.7333	1.7035	.34349	.4453
.7667	1.7210	.43075	.4438
.8000	1.7427	.54021	.4422
.8333	1.7696	.67729	.4407
.8667	1.8028	.84839	.4395
.9000	1.8433	1.06074	.4389
.9333	1.8923	1.32181	.4398
.9667	1.9503	1.63776	.4432
1.0000	2.0164	2.01539	.4509
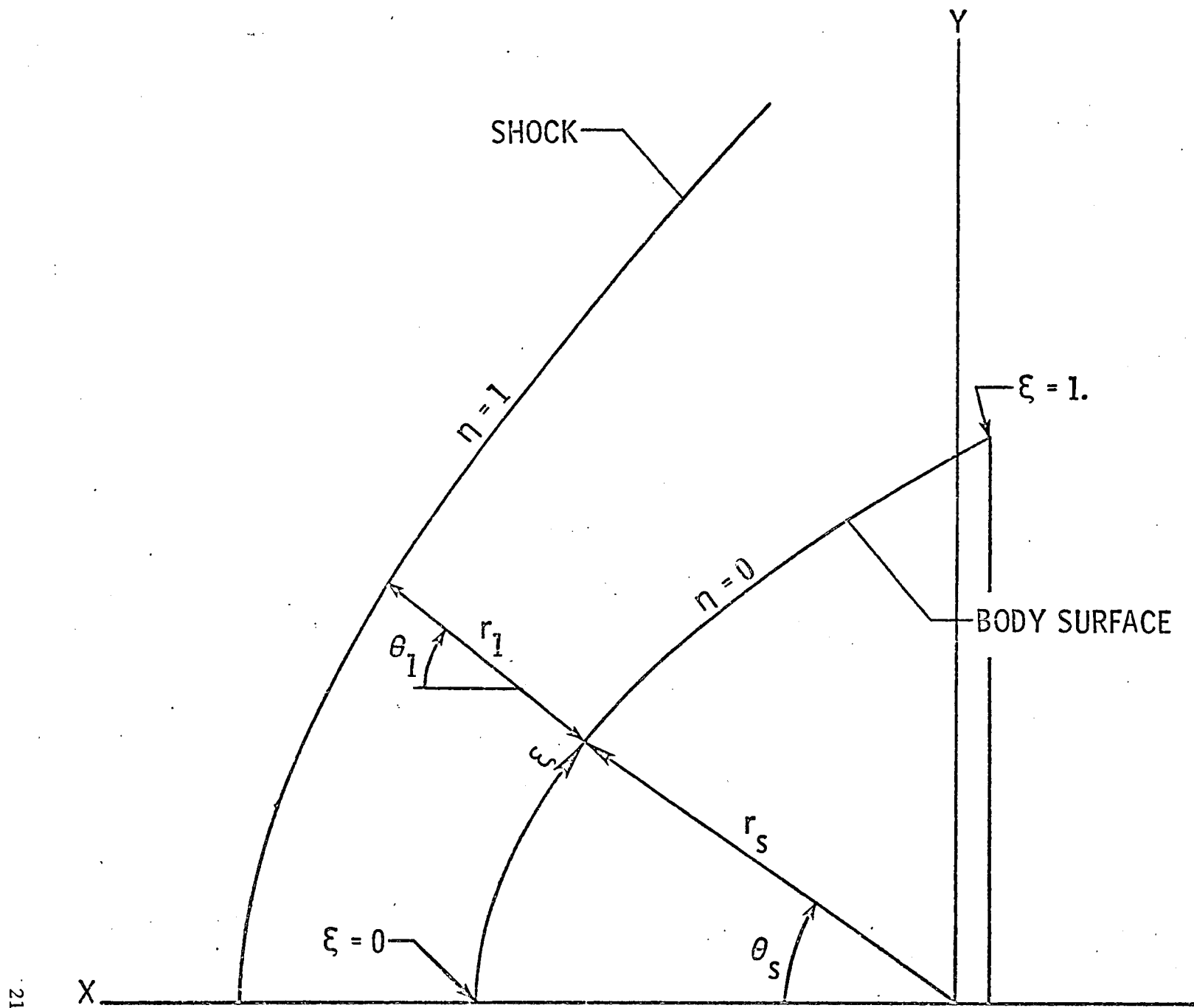
Fig. 1 Flow-field geometrical relationships.

SHOCK
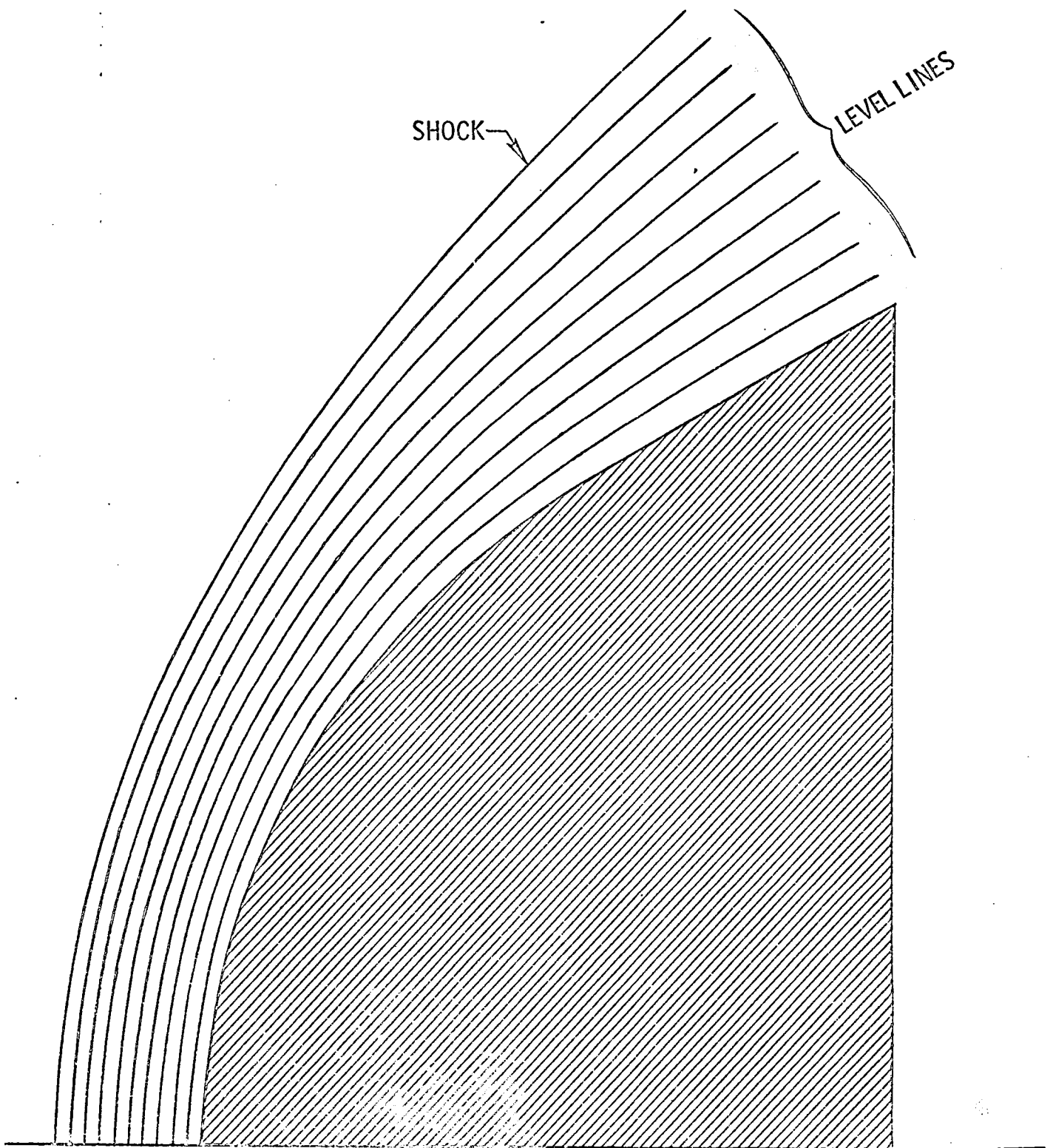
LEVEL LINES

Fig. 2 Level line construction.
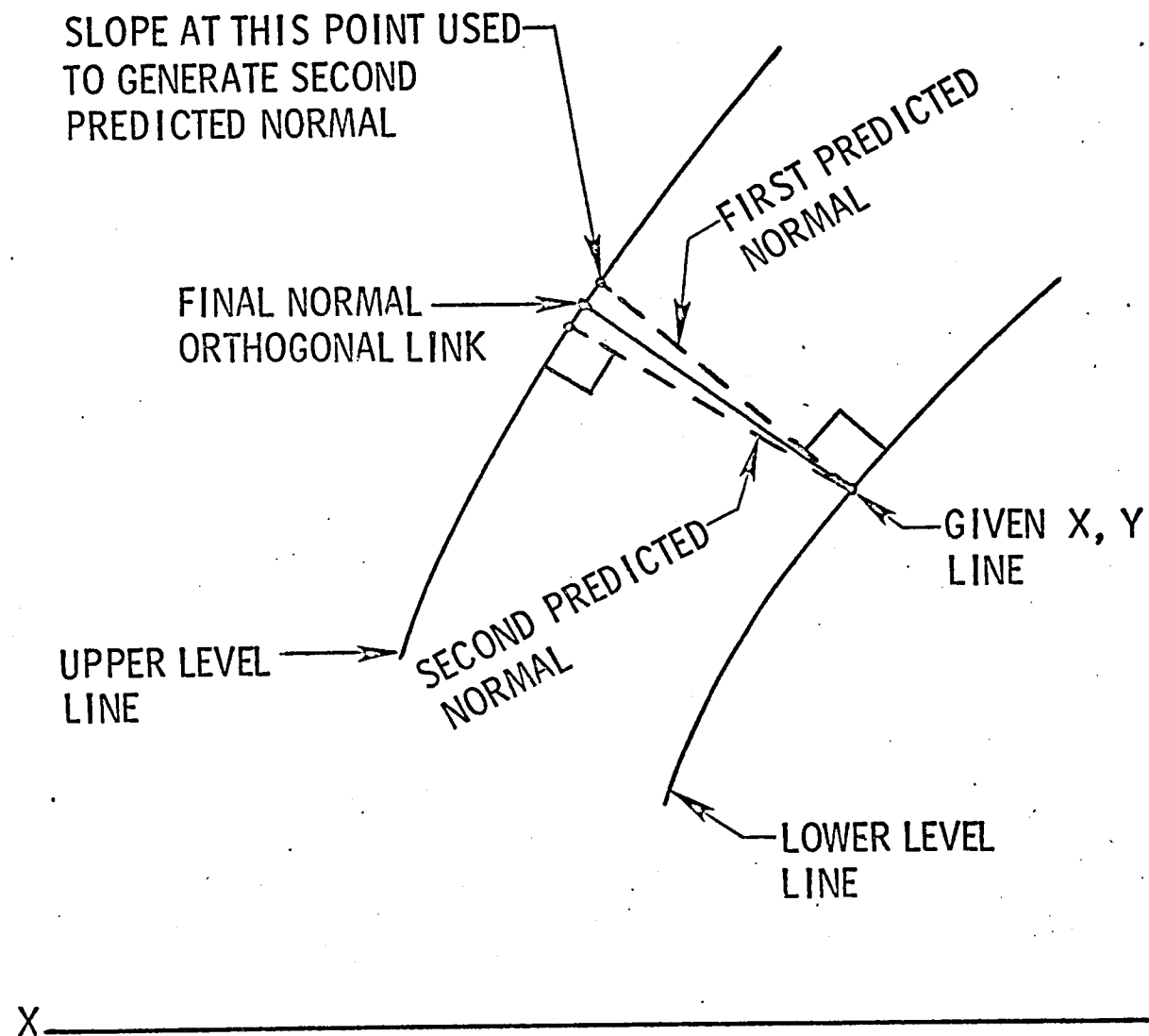
Fig. 3 Normal line construction technique.

SHOCK

LEVEL LINES

TYPICAL NORMAL
LINE CONSTRUCTED BY
"PREDICTOR - CORRECTOR"
PROCESS

24   Fig. 4 Typical coordinate mesh construction.
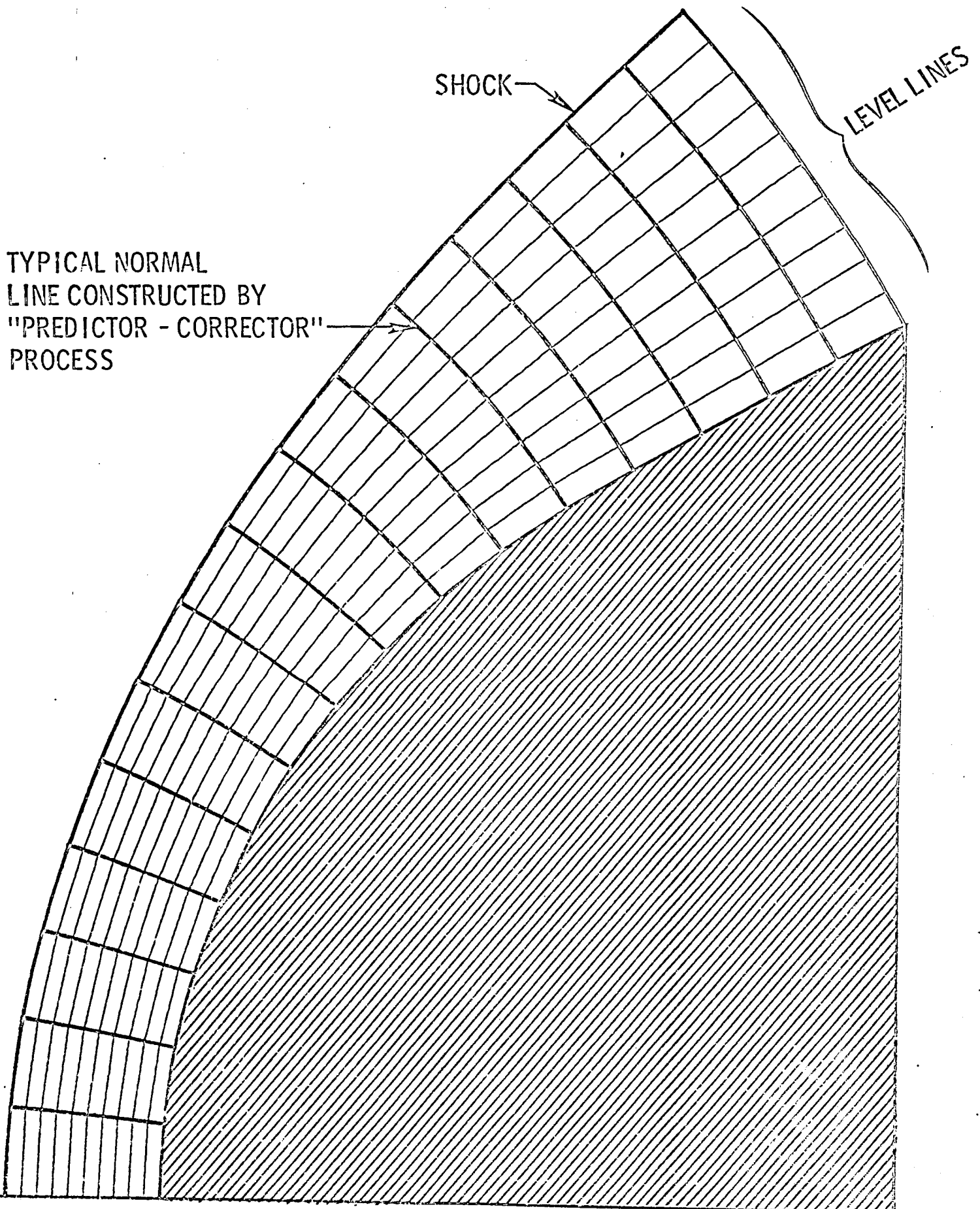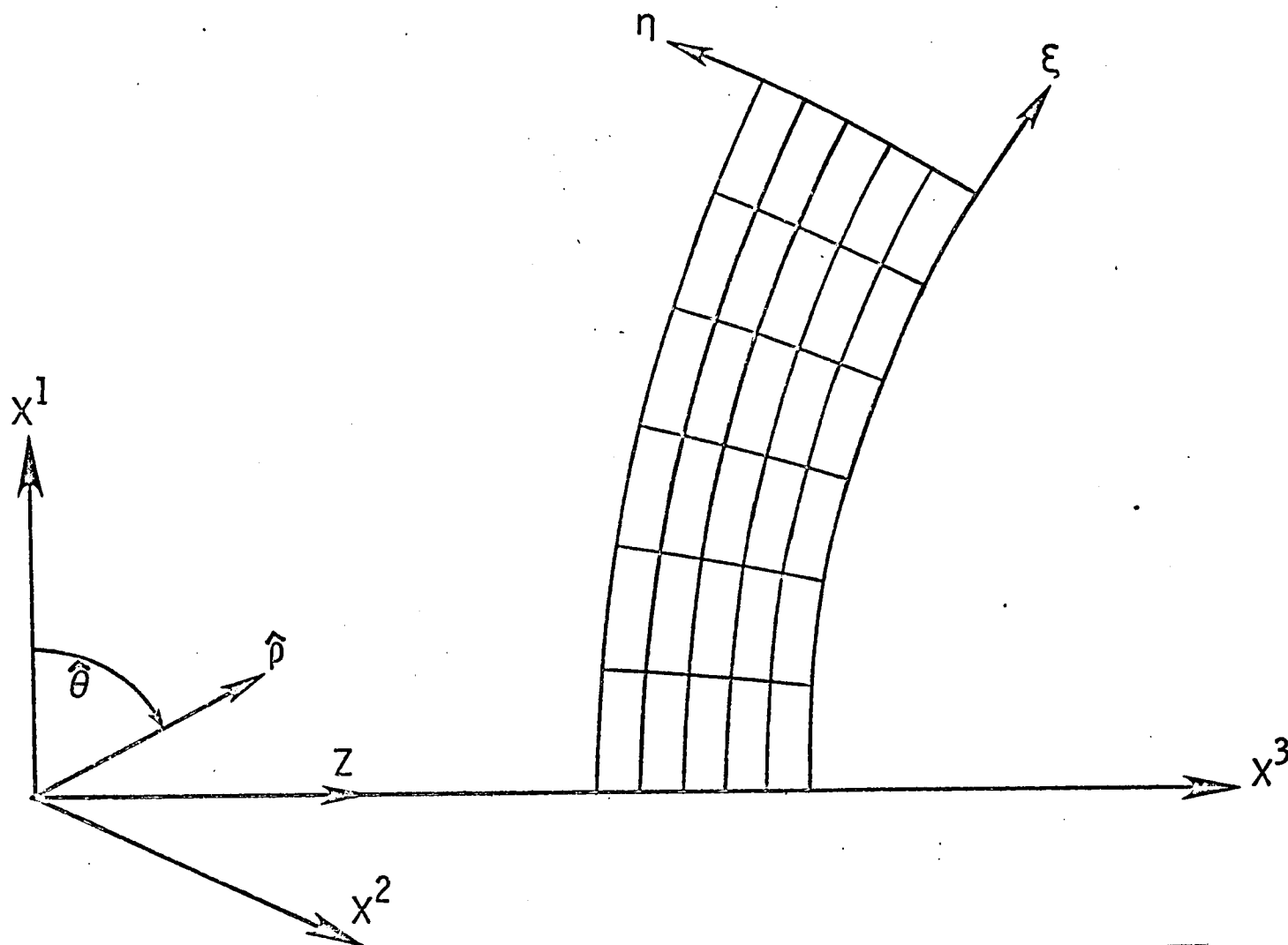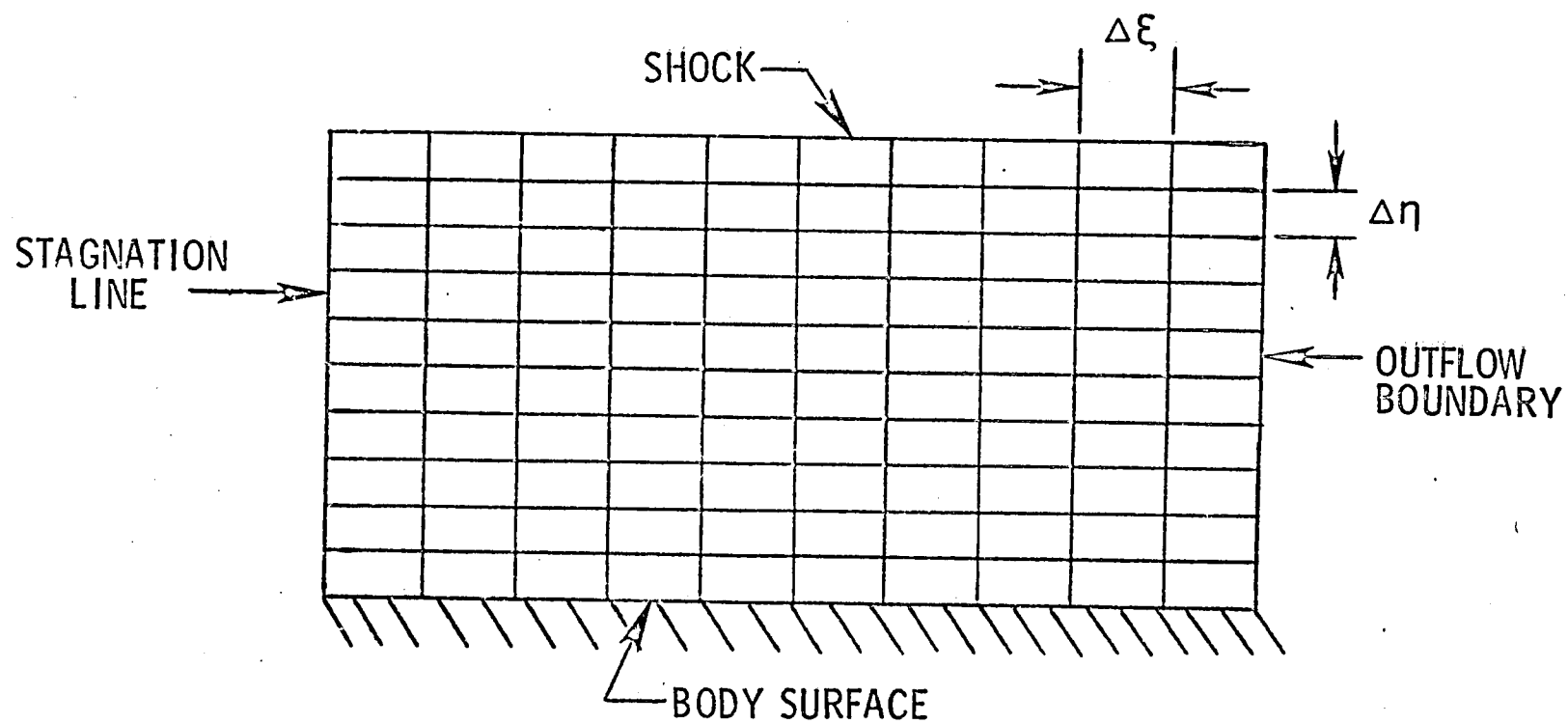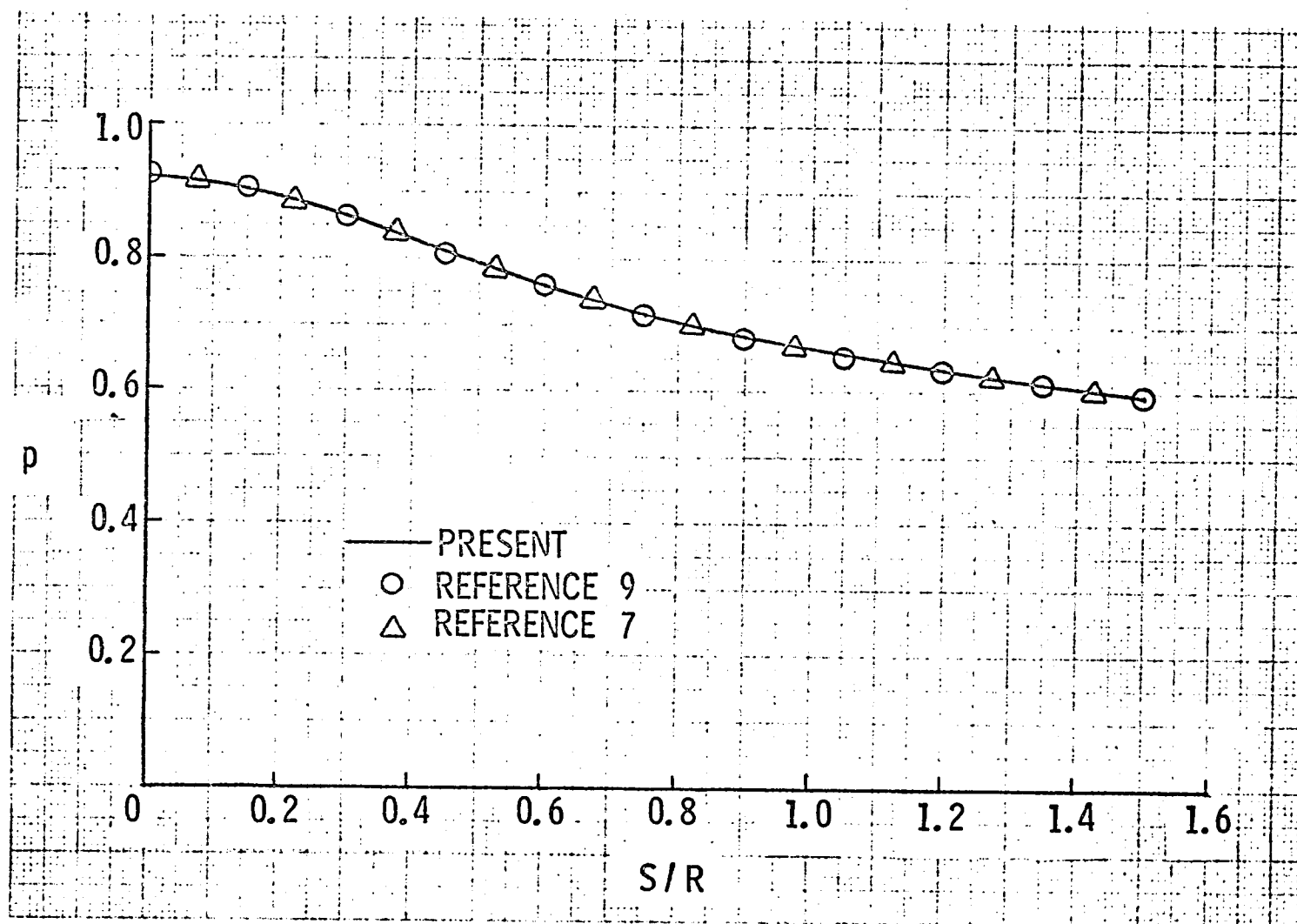
Fig. 5 Geometrical relationships for metrical coefficients.

Fig. 6 Computational mesh.

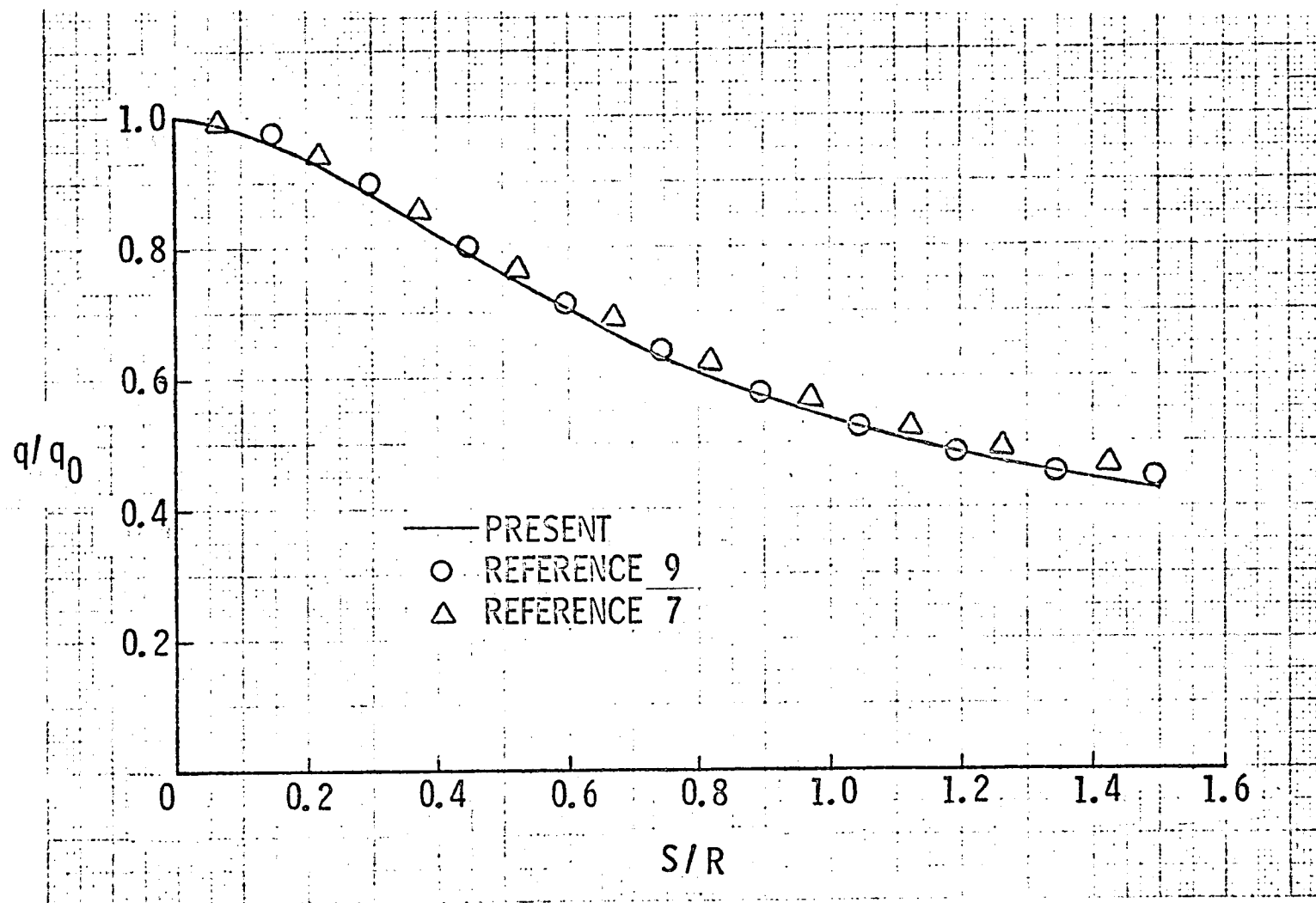Fig. 7 Computed pressure distributions for a 45° hyperboloid.
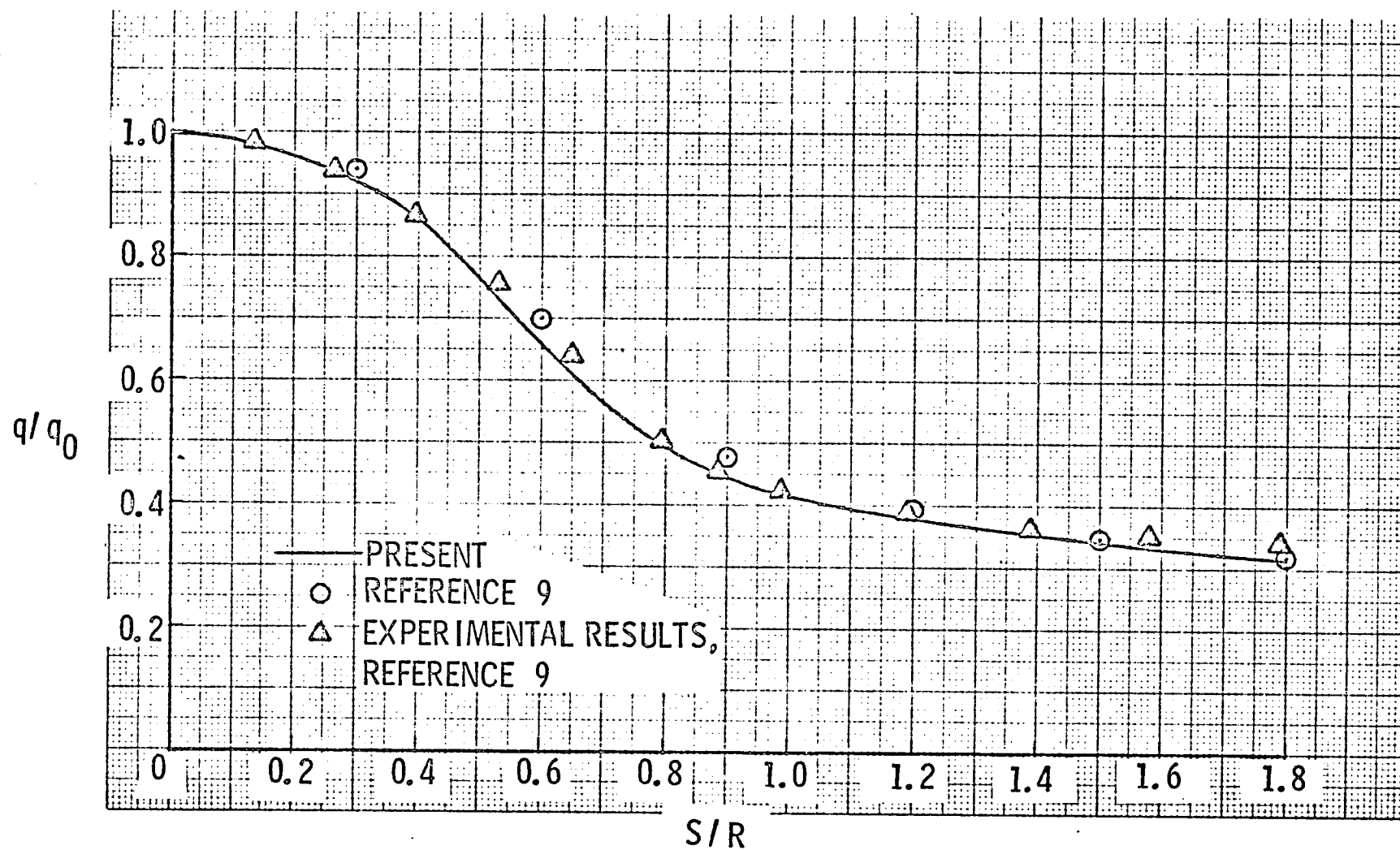
Fig. 8 Computed heat distributions for a 45° hyperboloid.

Fig. 9 Comparison of heat-transfer distributions for a 45° sphere cone.

40°

$X_0 = .4$

$X_0 = .3$

$X_0 = .2$

$X_0 = .1$

$X_0 = 0$
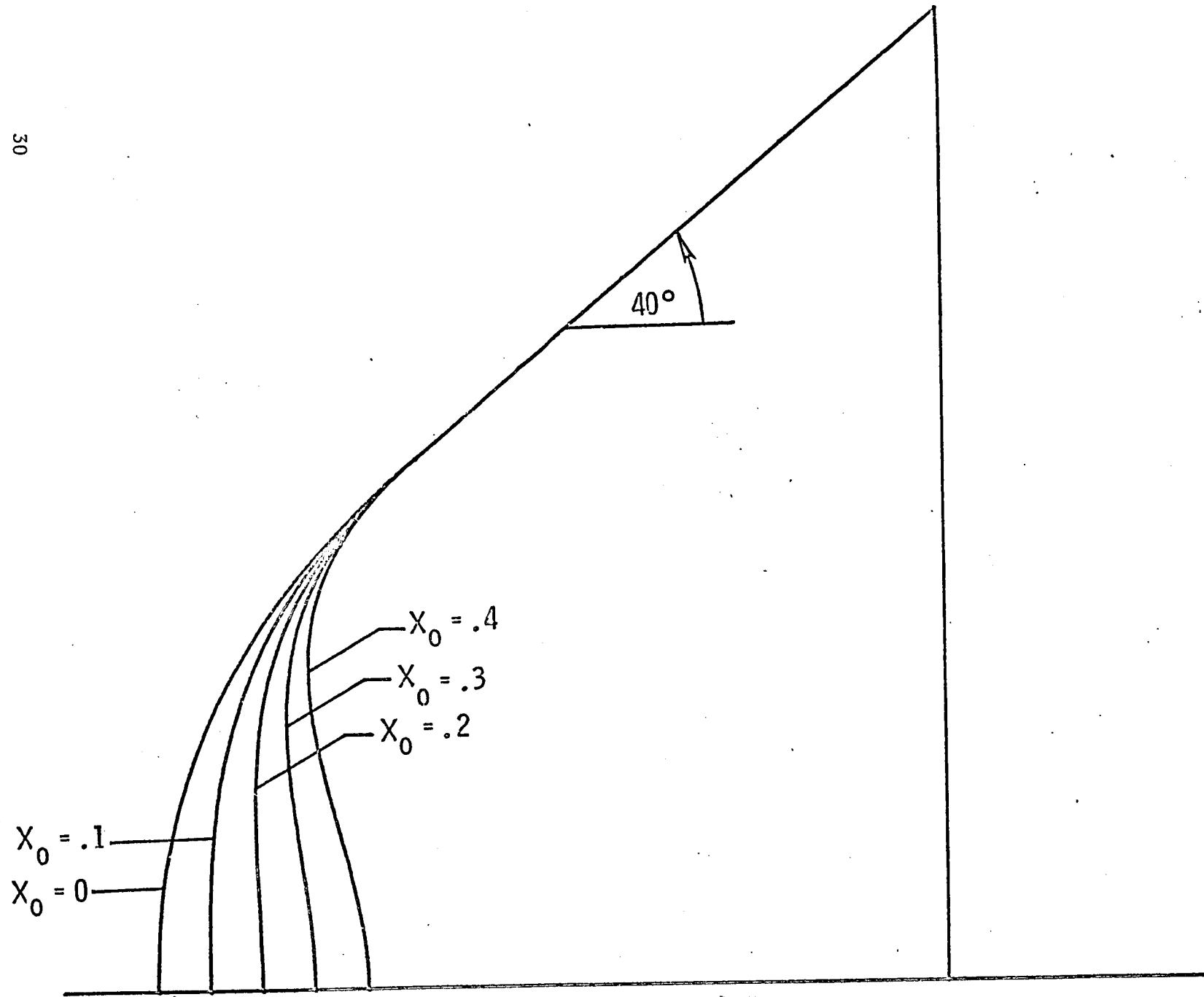
Fig. 10 Forebody shapes as a function of X_0.
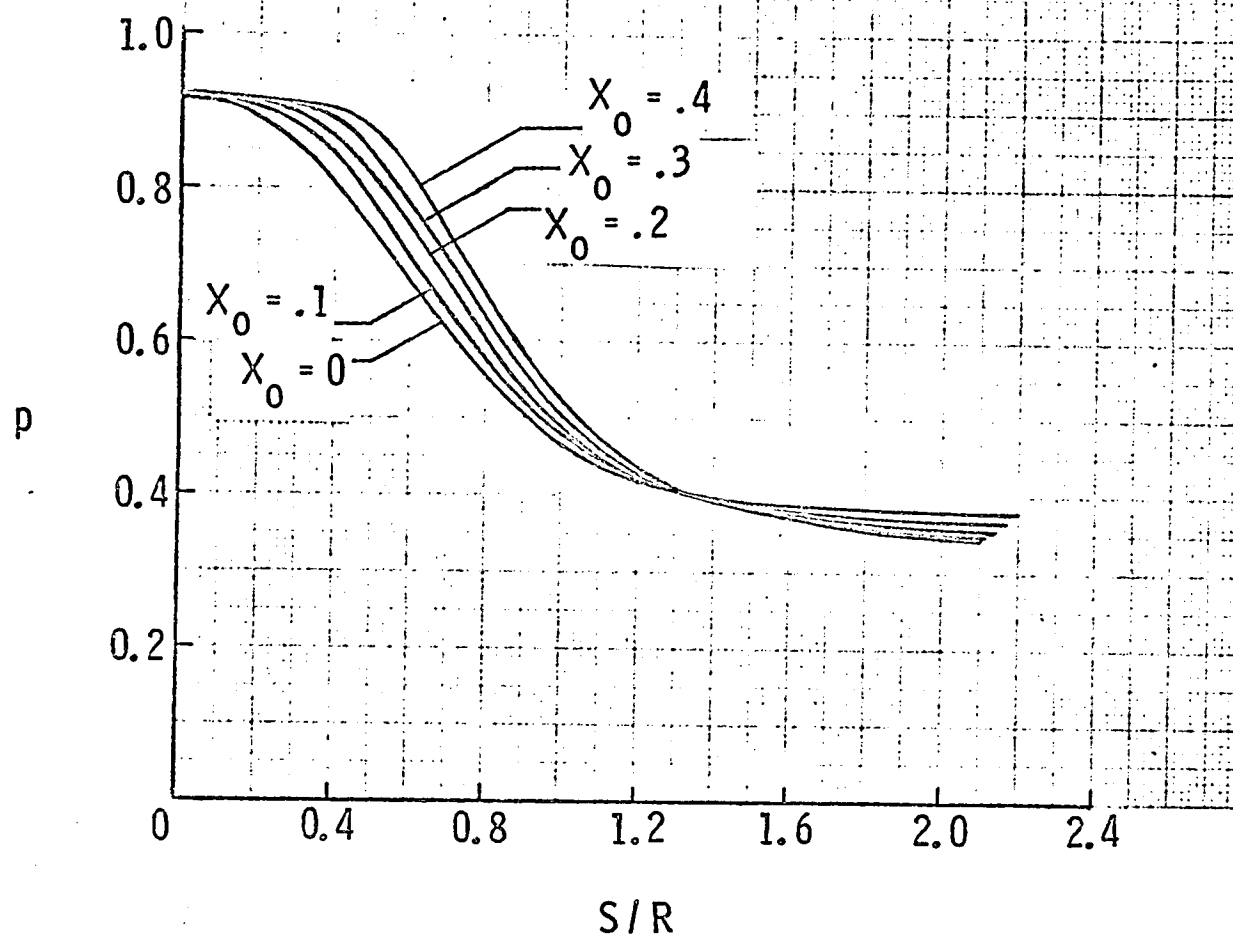
Fig. 11 Effect of nose blunting on the pressure distribution.
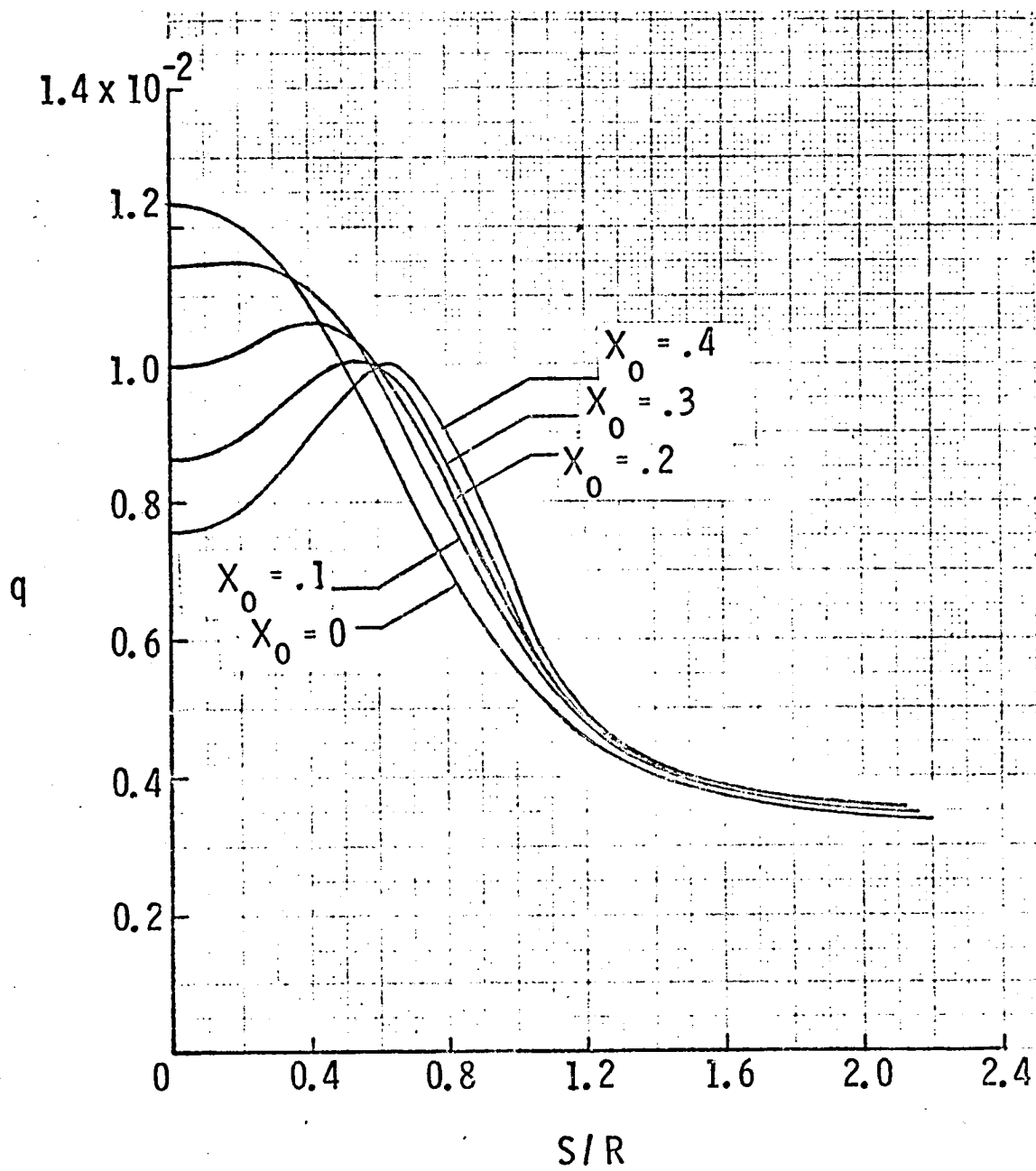
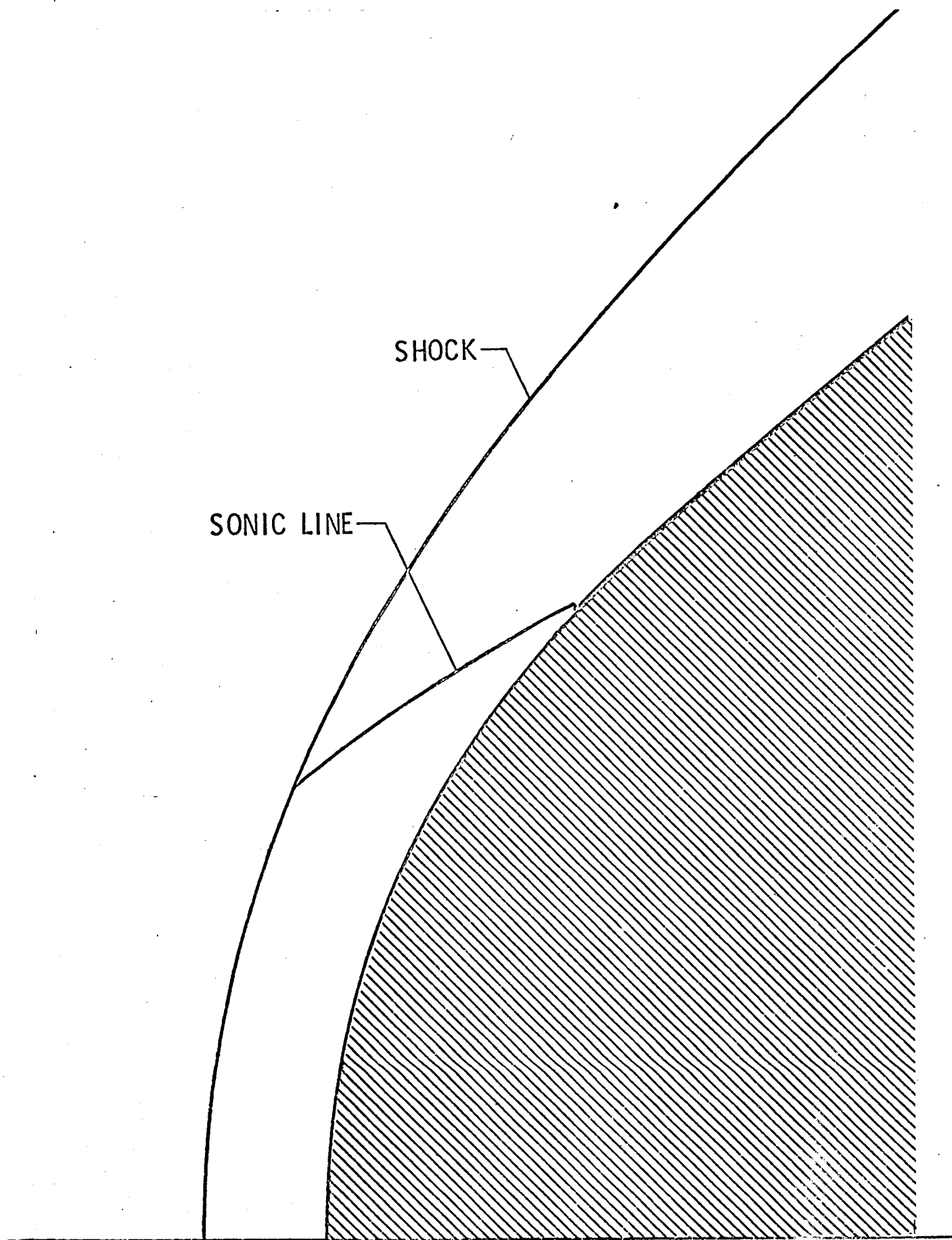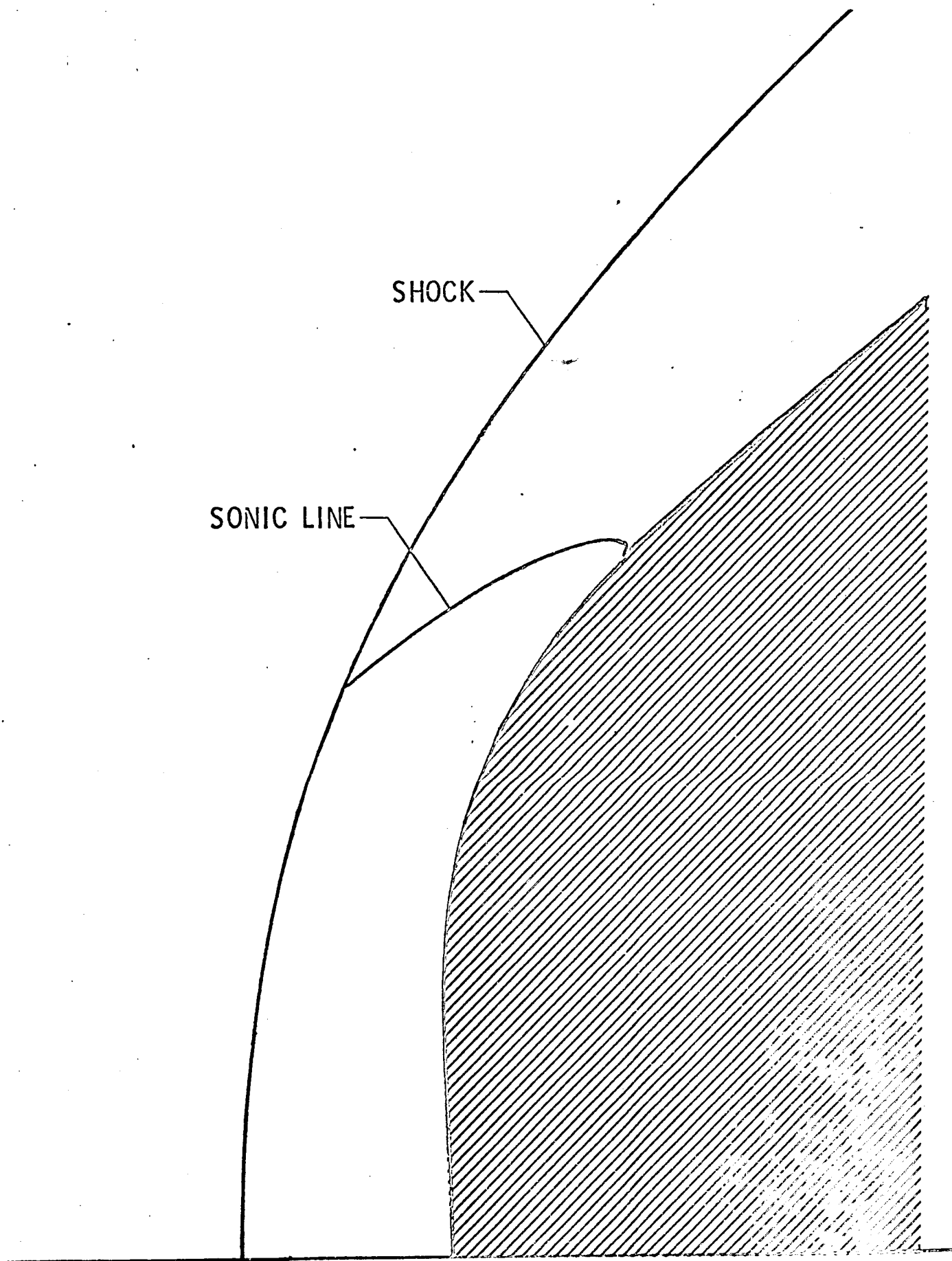Fig. 12 Effect of nose blunting on the heat-transfer distribution.

SHOCK

SONIC LINE

Fig. 13   Shock and sonic line for $X_0 = 0$.

SHOCK

SONIC LINE

Fig. 14   Shock and sonic line for $X_0 = .2$.
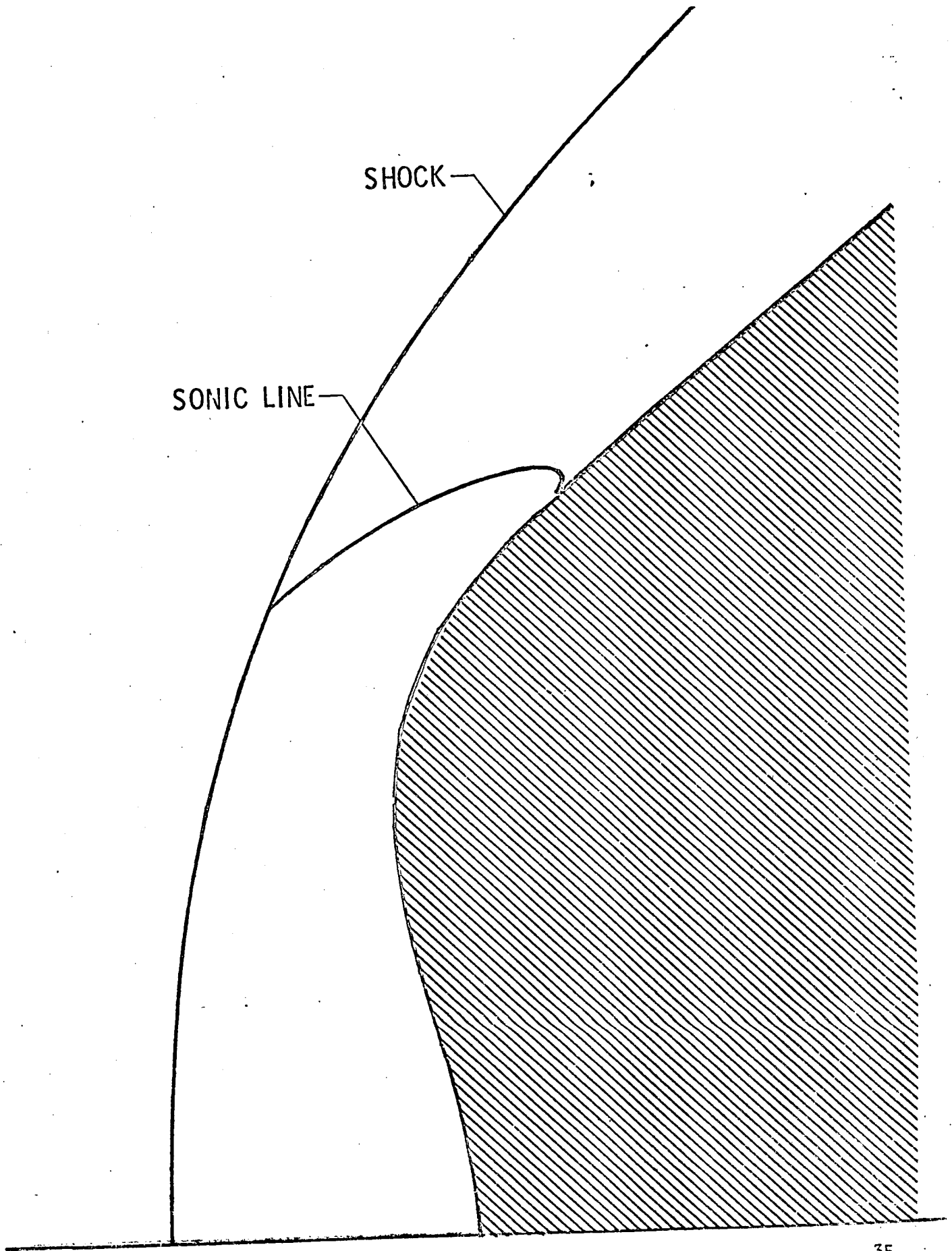
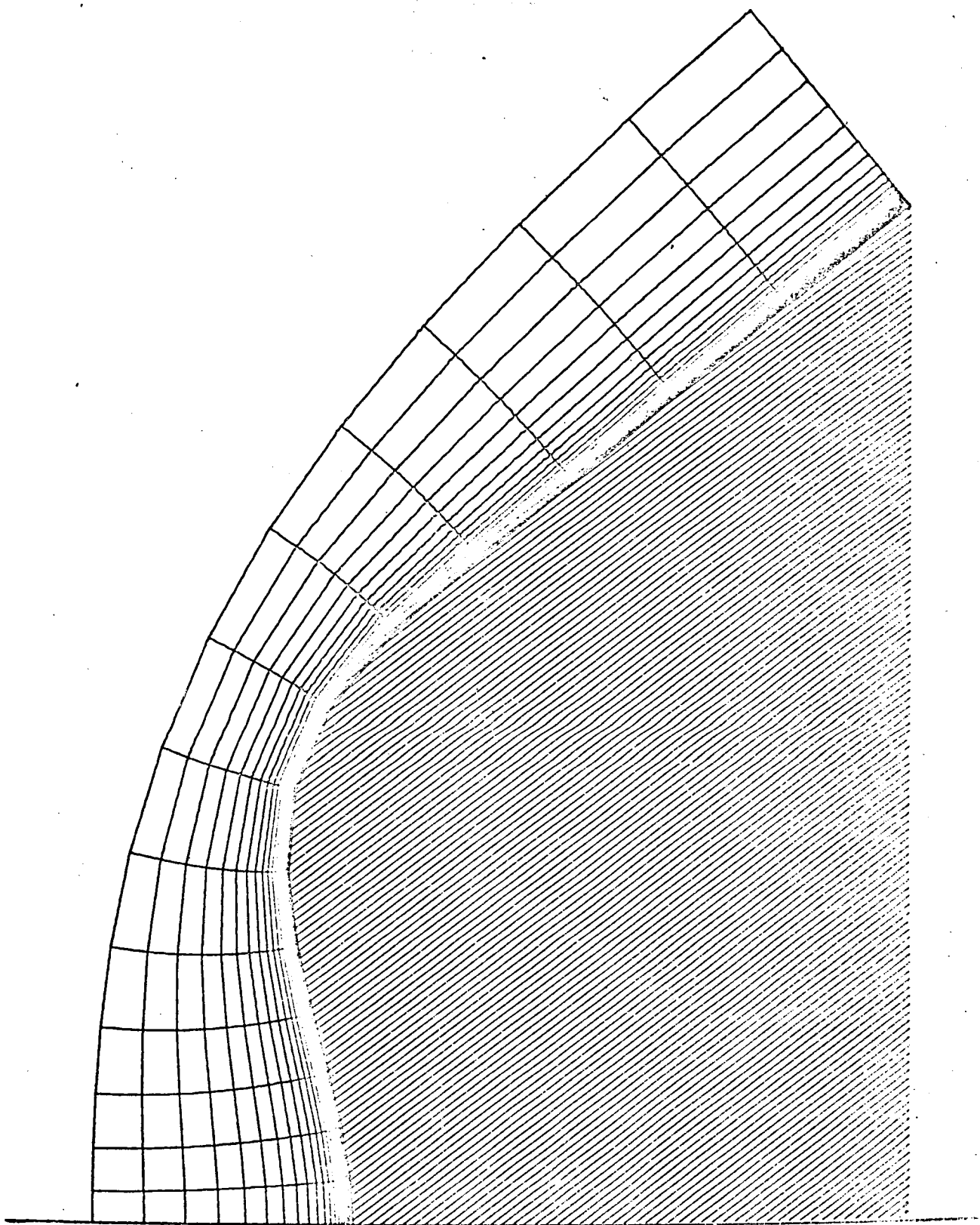SHOCK

SONIC LINE

Fig. 15 Shock and sonic line for $X_0 = .4$.

Fig. 16 Converged coordinate system for $X_0 = .4$.

1. Report No. NASA TM-81859	2. Government Accession No.	3. Recipient's Catalog No.
4. Title and Subtitle Viscous Compressible Flow About Blunt Bodies Using a Numerically Generated Orthogonal Coordinate System		5. Report Date July 1980
		6. Performing Organization Code
7. Author(s) R. A. Graves, Jr. and H. H. Hamilton II		8. Performing Organization Report No.
		10. Work Unit No. 506-51-13-01
9. Performing Organization Name and Address NASA Langley Research Center Hampton, Virginia 23665		11. Contract or Grant No.
		13. Type of Report and Period Covered Technical Memorandum
12. Sponsoring Agency Name and Address National Aeronautics and Space Administration Washington, DC 20546		14. Sponsoring Agency Code

15. Supplementary Notes

16. Abstract

   A numerical solution to the Navier-Stokes equations is obtained for blunt axisymmetric entry bodies of arbitrary shape in supersonic flow. These equations are solved on a finite-difference mesh obtained from a simple numerical technique which generates orthogonal coordinates between arbitrary boundaries. The governing equations are solved in time-dependent form using Stetter's improved stability three-step predictor-corrector method. For the present application, the metric coefficients were obtained numerically using fourth-order-accurate, finite-difference relations and proved to be totally reliable for the highly stretched mesh used to resolve the thin viscous boundary layer. Solutions are obtained for a range of blunt-body nose shapes including concavities.

17. Key Words (Suggested by Author(s)) Blunt Body Viscous Flow Computational Methods Navier Stokes Numerically Generated Coordinates	18. Distribution Statement Unclassified - Unlimited Subject Category 34

19. Security Classif. (of this report) Unclassified	20. Security Classif. (of this page) Unclassified	21. No. of Pages 36	22. Price* A03